Theory of anisotropic hybridization-broadened magnetic response in cerium and actinide systems

Gong-Jia Hu and Bernard R. Cooper
Department of Physics, West Virginia University, Morgantown, West Virginia 26506-6315
(Received 4 January 1993; revised manuscript received 12 July 1993)

Inelastic-neutron-scattering measurements on cerium and plutonium monopnictides, thought to have moderately delocalized f electrons, yield magnetic-excitation spectra with anisotropic dispersion; while reasonably sharp excitations have been observed only for USb and UTe among presumably more-delocalized uranium monopnictides and monochalcogenides. For UTe the broadening as well as the dispersion is quite anisotropic. We have now extended our previous theory for the magnetic behavior of hybridizing partially delocalized f-electron systems to include hybridization-induced relaxation effects in the magnetic response, and this work and results are reported in the present paper. Each partially delocalized f-electron ion is coupled by hybridization to the band sea; and this both leads to a hybridization-mediated anisotropic two-ion interaction giving magnetic ordering and also gives a damping mechanism, via the coupling to the band sea, for the excitations of the magnetically ordered lattice. This coupling also provides a strong renormalization of the magnetic-excitation energies obtained for the ionic lattice coupled by the two-ion interaction. To treat these effects on the magnetic response we have developed a formalism for calculating the dynamic susceptibility based on the projection-operator method developed by Mori and others. We have applied our model and theory to the behavior of CeSb, CeBi, PuSb, UP, UAs, and UTe; and excellent overall agreement with the wide range of unusual experimentally observed anisotropic magnetic-excitation behavior is obtained.

I. INTRODUCTION

The unusual magnetic behaviors of cerium and light actinide (uranium and plutonium) monopnictides and monochalcogenides with partially delocalized f electrons have been studied extensively.[1-9] The theory based on an anisotropic two-ion interaction, which arises from the hybridization of band electrons with f electrons, combined with the crystal-field interaction, has been successfully used to explain the main features of the anisotropic magnetic behaviors such as very large magnetic anisotropy,[1,2,6] complex magnetic phase diagrams[1,2,7] (see Table I), very small crystal-field splittings[6] (8 K in CeBi and 37 K in CeSb), and anomalous electrical resistivity and static susceptibility[10] behavior. The theory has also been used to understand the unusual magnetic excitation spectra for cerium and plutonium compounds.[3-5]

However, the magnetic excitation behaviors observed by the neutron-inelastic-scattering experiment[11-20] are still far from completely understood. For instance, for CeBi and CeSb a puzzling problem[12] is that, although the phase diagrams, the crystal-field splittings, and the ordering temperatures for the two materials are quite different, their low-temperature magnetic excitation behaviors are very similar: for both CeBi and CeSb the observed energy gap in the excitation spectrum at $\mathbf{q}=(000)$ is about 4.1 meV, the width of the observed neutron-scattering intensity peak is less than 1.0 meV, and the flat dispersion curve has energy minimum at the zone boundary $\mathbf{q}=(100)$ [wave vector $\mathbf{q}$ perpendicular to the ferromagnetic planes (001)]. For the uranium systems the situation is even more complicated. Despite the well-defined magnetic ordering (the pnicitide compounds are antiferromagnetic and the chalcogenide compounds are ferromagnetic, see Table I for the details), well-defined magnetic excitations are only observed for USb and UTe,[14] all the other compounds exhibit only a continuous spectrum of magnetic response. Furthermore, the dispersion and linewidth of the observed excitations in UTe are strongly anisotropic.[18] For $\mathbf{q}$ along the [111] direction both the excitation energy and the linewidth increase significantly on going from Γ to the zone boundary; while along the $[1\bar{1}0]$ direction the energy increase is much reduced, but the broadening increases rapidly.

Thus, the magnetic excitation behavior of plutonium and uranium monopnictides and monochalcogenides provides a wide range of unusual behavior which has been quite puzzling. We are now able to understand this behavior as well as the related behavior of the less delocalized cerium monopnictides.

In our earlier work,[1-9] we treated the unusual equilibrium and excitation magnetic behavior of cerium and light actinide monopnictides and monochalcogenides with partially delocalized f electrons by transforming the hybridization between the band electrons and the f electrons into resonant scattering from the correlated multiplet states of the ions. The exchange part of the scattering gives hybridization-mediated anisotropic two-ion interactions, physically corresponding to cooperative hybridization of the f-electron ions with the band sea, and treating the Hamiltonian containing both the two-ion interactions and crystal-field effects provides equilibrium behavior of the observed unusual anisotropic type. We then solved the equations of motion for the difference between the Hamiltonian and its mean-field approximation to obtain the dispersion of the magnetic excitations in the

0163-1829/93/48(17)/12743(16)/$06.00

TABLE I. Static magnetic properties of cerium and light actinide rocksalt structure compounds.

Compound	Lattice parameter (Å)	Transition temperature (K)	Magnetic structure	Easy direction	Ordered moment (μ_B)
CeSb	6.4	16.2	$T<8$ K, AF-IA $T>8$ K, AFP	⟨001⟩	2.0
CeBi	6.49	25.0	$T<12.5$ K, AF-IA $T>12.5$ K, AF-I	⟨001⟩	2.14
PuSb	6.24	85	$T<67$ K, F $T>67$ K, long-period AF	⟨001⟩	0.76
UAs	5.78	127	$T<64$ K, AF-IA double k	⟨110⟩	2.24
			$T>64$ K, AF-I single k	⟨001⟩	1.92
UP	5.59	125	$T<23$ K, AF-I double k	⟨110⟩	1.90
			$T>23$ K, AF-I single k	⟨100⟩	1.70
UTe	6.16	104	F	⟨111⟩	2.25

random-phase approximation (RPA).[2,5] Relaxation of the magnetic excitations was not included, and thus the excitations had infinite lifetimes. In this paper we present a relaxation theory for the magnetic excitations. We treat the hybridization of the f electrons with the non-f-band electrons as the main mechanism for the damping of the magnetic excitations. This hybridization, besides providing a mechanism for the indirect hybridization-mediated two-ion exchange leading to magnetic ordering, provides a mechanism for dissipating energy from the ionic magnetic lattice to the band sea as a sink, thereby damping the motion of that lattice. There is also a shift of energy, i.e., renormalization, of the RPA excitation energies calculated in the absence of damping.

By using the projection-operator method developed by Mori *et al.*,[21] we arrive at a formalism for calculating the imaginary part of the dynamic susceptibility which is proportional to the correlation function $S(\mathbf{q},\omega)$, the quantity that can be measured directly by the neutron-scattering experiments. We first consider CeBi and CeSb. The present theory answers the puzzling problem[12] of the very similar excitation spectra observed for these otherwise rather dissimilar antiferromagnets. We next apply the theory to PuSb, which has intraionic correlation effects since the Pu^{3+} ion is a system with five $5f$ electrons. This material has been well-studied experimentally.[20] However, the strongest challenge to the theory comes from the uranium systems (involving U^{3+} three $5f$-electron ions) since the f electrons in uranium systems are much more itinerant than those in corresponding cerium and plutonium compounds; and the site-based approach may be less valid for the uranium systems.[14] Thus, it is significant that after including the strong hybridization-induced relaxation, our site-based theory satisfactorily explains both the continuous spectra observed[14–17] in UAs and UP and the strongly anisotropic dispersion in[18] UTe.

In our phenomenological theory presented here, two independent types of hybridization-induced parameters are used. These are the single-site hybridization strength parameter $\mathcal{J}$ and the range parameters E_n characterizing the two-ion anisotropic exchange interactions giving magnetic ordering, respectively. (In the calculations we use values of $\mathcal{J}N(\varepsilon_F)$, where $N(\varepsilon_F)$ is the band density of states at the Fermi energy; and three range parameters E_1,E_2,E_3, which give the strengths of the interaction between an ion and its first-, second-, and third-nearest neighbors, are used.) According to the formalism established in our earlier work these two types of parameters are closely related.[2,6] However, at present, the first-principles calculations necessary to relate $\mathcal{J}$ and E_n have not been performed for most of the compounds we discuss. Therefore, we choose the values of $\mathcal{J}$ and E_n phenomenologically and independently. The values of $\mathcal{J}N(\varepsilon_F)$ are determined by fitting the experimentally observed linewidths at the Brillouin zone center. As we move from Ce^{3+} to Pu^{3+} then to U^{3+} these values are almost constant. (First-principles calculated values for the cerium compounds do provide a benchmark for comparison.) The values of E_n are basically determined by fitting the transition temperatures T_N and T_C; and in contrast to the $\mathcal{J}N(\varepsilon_F)$ behavior these values are about ten times larger for the uranium systems than for the corresponding cerium systems, with the values of E_n for PuSb being between these extremes. In Sec. IV, we will discuss this contrast.

The organization of the present paper is as follows. In Sec. II, we briefly review the theory for the hybridization-mediated two-ion interaction and the calculation of the undamped magnetic excitations. The relaxation theory for calculating the dynamic susceptibility is described in Sec. III. Application of the theory to cerium, plutonium, and uranium systems and discussion of the calculated results are given in Sec. IV. Finally, in Sec. V, a summary of our results and conclusions is given.

II. THEORETICAL BACKGROUND

In this section we briefly review the model for hybridization-mediated interionic coupling in f^N systems ($N=1,3,5$ for Ce^{3+}, U^{3+}, Pu^{3+}, respectively) and the equations-of-motion theory for the magnetic excitations. Special attention will be paid to the direct band-f scattering term in the Hamiltonian when transformed to resonant scattering form. Wills and Cooper[6] have shown that this direct interaction term is the key to understanding the unusual deviation of the measured paramagnetic crystal-field splittings from expected values for CeBi and CeSb. Now we show that it is also responsible for a renormalization of the band states, which causes a broadening of the f levels and hence gives rise to a leveling off of the value of the single-site hybridization strength parameter $\mathscr{J}$, instead of a continuous rise as expected from our earlier work as the f levels approach the Fermi level for U^{3+} systems.

A. Model Hamiltonian

Following Ref. 2, we use the ionic (site-based) model for describing these systems. The model Hamiltonian is derived from the Anderson model in describing the hybridization between the f and the band electrons. The Hamiltonian for a single ion mixing with a sea of band electrons is

$$H_A=H_1+H_2 , \tag{2.1}$$

$$H_1=\sum_{\mathbf{k},M}\varepsilon_{\mathbf{k}}n_{\mathbf{k},M}+\sum_M \mathscr{E}_M n_M+\frac{U}{2}\sum_{M,M'} n_M n_{M'} , \tag{2.2}$$

$$H_2=\sum_{\mathbf{k},M}(V_{\mathbf{k},M}C^\dagger_{\mathbf{k},M}C_M+V^*_{\mathbf{k},M}C^\dagger_M C_{\mathbf{k},M}) , \tag{2.3}$$

where $\mathbf{k}$ is the wave vector of the band electrons, M and M' are the magnetic quantum numbers of the ionic states (the localized states of the f electrons) and of the $l=3(f)$ components of the band electrons when expressed in spherical waves about the site in question; $\varepsilon_{\mathbf{k},M}$ are the band electron energies; $\mathscr{E}_M$ are the configuration energies for the ion; U is the Coulomb correlation energy difference between different configurations; $V_{\mathbf{k},M}$ is the strength of the hybridization potential. Values of $\varepsilon_{\mathbf{k}}$, $\mathscr{E}_M$, and U are measured relative to the Fermi energy ε_F. $n_{\mathbf{k}M}$ and n_M denote the number operators, while $C_{\mathbf{k}M}$ and C_M denote destruction operators for the band and ionic states, respectively. Upon applying the Schrieffer-Wolff transformation,[22-25] a canonical transformation $e^S H_A e^{-S}$ designed to diagonalize H_A through first order in H_2 with S defined so that $[S,H_1]=-H_2$, the hybridization Hamiltonian for the case of an f^N configuration can be written as[25]

$$H^{(2)}_{\rm ex}=H_{\rm ex}+H_{\rm dir}+H_f , \tag{2.4}$$

$$H_{\rm ex}=-\sum_{\mathbf{k},\mathbf{k}'}\sum_{M,M'}[j_N^{M,M'}(\mathbf{k},\mathbf{k}') - j_{N-1}^{M,M'}(\mathbf{k},\mathbf{k}')]C^\dagger_{\mathbf{k},M'}C_{\mathbf{k},M}C^\dagger_M C_{M'} , \tag{2.5}$$

$$H_{\rm dir}=\sum_{\mathbf{k},\mathbf{k}',M}\left[j_N^{MM'}(\mathbf{k},\mathbf{k}')\left[\sum_{M'\neq M}n_{M'}+1-N\right] - j_{N-1}^{MM'}(\mathbf{k},\mathbf{k}')\left[\sum_{M'\neq M}n_{M'}-N\right]\right]C^\dagger_{\mathbf{k}',M}C_{\mathbf{k},M} , \tag{2.6}$$

$$H_f=-\frac{1}{2}\sum_{\mathbf{k},\mathbf{k}'}\sum_{M\neq M'}[j_N^{M,M'}(\mathbf{k},\mathbf{k}')-j_{N-1}^{MM'}(\mathbf{k},\mathbf{k}')] \times(C^\dagger_{\mathbf{k}'M'}C^\dagger_{\mathbf{k}M}C_M C_{M'} + C_{\mathbf{k}'M'}C_{\mathbf{k}M}C^\dagger_M C^\dagger_{M'}) , \tag{2.7}$$

with the single-site exchange parameter j given by

$$j_N^{M,M'}(\mathbf{k},\mathbf{k}')=\frac{V_{\mathbf{k},M}V^*_{\mathbf{k}'M'}}{2}\left[\frac{1}{\varepsilon_{\mathbf{k}}-\mathscr{E}_M-NU}+\frac{1}{\varepsilon_{\mathbf{k}'}-\mathscr{E}_{M'}-NU}\right] . \tag{2.8a}$$

For cerium systems, since U (of the order of 6 eV) (which leads to a definite $4f^1$ configuration) is much larger than the energy of the f levels $\mathscr{E}_M$ ($\sim$2 eV with respect to the Fermi energy), while $\mathscr{E}_M$ is much larger than the crystal-field splitting (of the order of 0.01 eV), we neglect the difference between $\mathscr{E}_M$ and $\mathscr{E}_{M'}$ and take them equal to $\mathscr{E}_f$. Considering that most scattering occurs in the vicinity of the Fermi energy, we take $\varepsilon_{\mathbf{k}}=0$. Then the parameter j becomes

$$j_1^{MM'}(\mathbf{k},\mathbf{k}')=\frac{|V_{\mathbf{k}M}|^2}{\mathscr{E}_f+U} , \tag{2.8b}$$

and the single-ion hybridization strength parameter is given by

$$\mathscr{J}^{MM'}(\mathbf{k},\mathbf{k}')=j_1^{MM'}(\mathbf{k},\mathbf{k}')-j_0^{MM'}(\mathbf{k},\mathbf{k}') =\frac{|V_{\mathbf{k}M}|^2U}{\mathscr{E}_f(\mathscr{E}_f+U)}\simeq\frac{|V_{\mathbf{k}M}|^2}{\mathscr{E}_f} . \tag{2.8c}$$

To extend our theory to the systems with more than one f electron per ion, the basic assumption[2,5] is that the single-site scattering event consists of a one-electron (out of the many-electron ionic state) exchange only; all the quantum numbers of all the other electrons in the ion remain the same; and the scattering, being a single-electron process, does not affect the other electrons. (The many-particle excitation effects will be considered below in treating the relaxation effects.) Thus, only one electron at a time hybridizes with the band electrons, in spite of the fact that there is more than one f electron in the ionic system. In other words, $\sum_M n_M=1$, and we should take $N=1$ in all the equations [Eqs. (2.4)–(2.8)] no matter how many f electrons there are. In plutonium systems, $Pu^{3+}(5f^5)$, the Coulomb integral $U\sim$4–5 eV and $\mathscr{E}_f\sim$2 eV; and since the relative sizes are not that much changed from $Ce^{3+}(4f^1)$, it is appropriate to assume that our theory for Ce^{3+} (hence all the equations) can also be applied to Pu^{3+} systems. However, for $U^{3+}(5f^3)$ systems, due to the smaller Coulomb configuration energy U

($\sim$2–3 eV) the fluctuations between configurations become important. Furthermore, the smaller f energy (f levels are located $\sim$0.5 eV below the Fermi energy) gives a large hybridization potential $V_{\mathbf{k}M}$ and makes U^{3+} systems more itinerant than Ce^{3+} and Pu^{3+} systems. Recalling that in our previous work $V_{\mathbf{k}M}$ was treated as the smallest perturbation compared to the other energies, such as U, $\mathcal{E}_f$, and the spin-orbit splitting, it seems questionable to apply the theory to systems like U^{3+} with much larger $V_{\mathbf{k}M}$. In the present work, we have examined the change in hybridization as the f levels approach the Fermi energy, and have seen that, despite these important changes in behavior, the basically ionic (site-based) picture still provides a useful description of relaxation effects. Thus, we continue to neglect the fluctuations between configurations, and still treat $V_{\mathbf{k}M}$ as a perturbation for $U^{3+}(5f^3)$ systems. We choose UAs, UP (which have smaller lattice parameters and presumably have the larger $V_{\mathbf{k}M}$), and UTe (with larger lattice parameter and hence presumably smaller $V_{\mathbf{k}M}$) as examples to test our theory, and compare our results with experiment for these materials.

As shown by Eqs. (2.4)–(2.7), the net effect of the Schrieffer-Wolff transformation, to second order in H_2, is to replace the band-f hybridization interaction term in the Hamiltonian by a direct scattering term $H_{\rm dir}$, an exchange scattering term $H_{\rm ex}$, and an f-f band term H_f. As stated above, we neglect the fluctuations between configurations for the f-electron ions. Therefore, we neglect the f-f banding term H_f, which creates or destroys two f electrons on the ion. Then the exchange scattering Hamiltonian $H_{\rm ex}$ given in Eq. (2.5), treated in second-order perturbation theory on band states according to the theory developed by Cooper and Siemann,[1] results in an indirect hybridization-mediated anisotropic interaction between f states on two ions, which is generically related to the Ruderman-Kittel-Kasuya-Yosida[26] (RKKY) interaction; but where the interaction with the band electrons is through the orbital rather[1,2,26(a)] than the spin part of the f-electron moment.

Since the band states enter the overall magnetic response as probed by the scattered neutrons globally, the dependence of $j^{MM'}(\mathbf{k},\mathbf{k}')$ on $\mathbf{k}$ and $\mathbf{k}'$ can be neglected. Thus, for simplifying the calculation, following Coqblin and Schrieffer,[24] in Eq. (2.8) we neglect the dependence of $j^{MM'}(\mathbf{k},\mathbf{k}')$ on $\mathbf{k}$ and $\mathbf{k}'$, and take a cutoff energy D independent of M and M', so that $j^{MM'}=0$ if $|\varepsilon_{\mathbf{k}}|$ or $|\varepsilon_{\mathbf{k}'}|>D$; where the cutoff energy D is chosen to be of the order of the mean value of the $\mathcal{E}_M$. (This procedure is consistent with the phenomenological framework used in the present work in treating the equilibrium magnetic ordering. In those treatments of the equilibrium magnetic ordering where we have included detailed band behavior,[6,26(b),26(c)] we have found only quantitative refinement of the results using this approximation.) Then the exchange scattering Hamiltonian $H_{\rm ex}$ takes the form

$$H_{\rm ex}=-\mathcal{J}\sum_{\mathbf{k},\mathbf{k}'}\sum_{M,M'}C^{\dagger}_{\mathbf{k}',M'}C_{\mathbf{k},M}C^{\dagger}_{M}C_{M'}\ , \tag{2.9}$$

and the two-ion exchange interaction takes the form[2]

$$H_{\rm two}=-\sum_{\mu,\nu,\epsilon,\sigma}\mathcal{T}^{\epsilon\sigma}_{\mu\nu}(\mathbf{R}_{i,j})L^{(i)}_{\mu\nu}L^{(j)}_{\epsilon\sigma}\ , \tag{2.10}$$

where μ,ν,ϵ,σ refer to the ionic states, and transition operators $L_{\mu\nu}$ are defined as

$$L_{\mu\nu}=|\mu\rangle\langle\nu|\ , \tag{2.11}$$

$\mathbf{R}_{ij}$ is the displacement between sites i and j, and

$$\mathcal{T}^{\epsilon\sigma}_{\mu\nu}(\mathbf{R}_{ij})=E_{ij}B^{\epsilon\sigma}_{\mu\nu}(\theta)e^{-i(\mu-\nu+\epsilon-\sigma)\phi} \tag{2.12}$$

with

$$B^{\epsilon\sigma}_{\mu\nu}(\theta)=\sum_{MM'}\sum_{NN'}\mathcal{J}^{NN'}_{MM'}d_{\mu M'}(\theta)d_{\nu M}(\theta)d_{\epsilon N}(\theta)d_{\sigma N'}(\theta)\ . \tag{2.13}$$

Here indices, M, M', N, and N' are summed over all possible M (magnetic quantum number) values for the ground-state multiplet of the ion; θ and ϕ are the polar and azimuthal angles of the interionic axis $\mathbf{R}_{ij}$ with respect to axis of quantization chosen along a cube edge direction the crystal; $d_{\alpha\beta}(\theta)$ is the rotational transformational matrix as is conventionally defined;[27] the E_{ij} are range functions giving the strength of the exchange interactions and are treated as phenomenological parameters with E_n giving the strength of the interaction with the nth nearest neighbors, and

$$\mathcal{J}^{NN'}_{MM'}=\sum_{m,m'}\Lambda^{MM'}_{mm'}\Lambda^{NN'}_{mm'}\ , \tag{2.14}$$

where m and m' are the magnetic quantum numbers of one electron within the ion. The Λ are defined in terms of the scattering coefficients $A^{MM'}_{mm'}$ as

$$\Lambda^{MM'}_{mm'}=A^{MM'}_{mm'}-\frac{\delta_{mm'}\delta_{MM'}}{2J+1}\sum_{N}A^{NN}_{mm}\ . \tag{2.15}$$

The scattering coefficient $A^{MM'}_{mm'}$ corresponds to first adding (removing) a band (localized) electron with magnetic quantum number m to (from) the ion state $|J,M'\rangle$ to produce an f^{N+1} (f^{N-1}) intermediate state, and then removing (adding) a localized (band) electron with magnetic quantum number m' to give the final state $|J,M\rangle$. The detailed description of the evaluation of $A^{MM'}_{mm'}$ and an example of its calculation are given in Refs. 5 and 2 and 4, respectively. It has been shown[1,2] that, in the limit of large $\mathbf{R}_{ij}$, the dominant single-site scattering processes in the two-ion interactions are those involving f electrons in the $m=\pm\frac{1}{2}$, $m_l=0$, $m_s=\pm\frac{1}{2}$ states, and for the ionic systems containing more than one f electron, the next-to-dominant scattering channels (single-site scattering processes involving f electrons with $m=\pm\frac{1}{2}$, $m_l=\pm1$, $m_s=\mp\frac{1}{2}$) may be critical[5] for determining the correct polarization in magnetically ordered systems.

The direct scattering term $H_{\rm dir}$ given in Eq. (2.6) has been used[6] to explain the anomalous small crystal-field splittings in CeBi and CeSb. The diagonal ($\mathbf{k}=\mathbf{k}'$) elements in $H_{\rm dir}$ give a shift in the f-state energy levels. For the rocksalt structure Ce^{3+} monopnictides, treating $H_{\rm dir}$ as a perturbation on the bare crystal-field levels, Wills and Cooper[6] have shown that the hybridization between

band states and f states affects the Γ_8 quartet of the Ce^{3+} $4f_{5/2}$ manifold more strongly than the Γ_7 doublet of that manifold. The difference in band-f hybridization between the Γ_7 doublet and the Γ_8 quartet changes the splitting of the bare crystal-field levels. They calculated the relative shifts in the $\Gamma_7-\Gamma_8$ splitting for CeBi and CeSb and found that the calculated change in the crystal-field splitting gives excellent agreement with the deviation of the measured crystal-field splitting from values expected from extrapolation from other rare-earth monopnictides. For simplifying the calculations we treat this hybridization-induced anomalous crystal-field splitting by choosing the so-called hybridization-dressed crystal-field parameter [B_4, defined below in Eq. (2.21)] to fit the experimental behavior.

In addition to the hybridization dressing effect on the crystal-field splitting, another related effect that should also be included in the theory is the renormalization of the single-site hybridization strength parameter $\mathscr{J}$ caused by the direct scattering term in the Hamiltonian. When we diagonalize the Hamiltonian $(H_1+H_{\rm dir})$ by a transformation[28]

$$C_s^\dagger=\sum_s \langle s|k\rangle C_k^\dagger \ , \tag{2.16}$$

where $|s\rangle$ denotes the scattered state, the nondiagonal ($\mathbf{k}\neq\mathbf{k}'$) elements in the direct scattering term $H_{\rm dir}$ give rise to a renormalization of the band states. Following Kondo,[28] this yields a phase shift of the band states scattered by the f states:

$$\tan\delta(\varepsilon_s)=-\frac{\pi V\rho(\varepsilon_s)}{[1-VP\int\rho(\varepsilon_k)/(\varepsilon_s-\varepsilon_k)d\varepsilon_k]} \ , \tag{2.17}$$

where P denotes the principal value of the integral, $\rho(\varepsilon_s)$ is the density of band states, and V is the strength of the hybridization potential defined by Eq. (2.3).

Toulouse and Coqblin[29] have shown that this phase shift yields a renormalization factor of $\mathscr{J}$ given by

$$R=\left|\sum_k \langle s|k\rangle\right|^2=\frac{1}{\pi\rho(\varepsilon_F)}\left|\frac{d\delta(\varepsilon_F)}{dV}\right| \ . \tag{2.18}$$

Combining Eqs. (2.17) and (2.18) we have

$$R=\frac{\varepsilon_f}{\Gamma^2+(\mathscr{E}_f+\gamma)^2} \ , \tag{2.19}$$

where $\Gamma=\pi V^2\rho(\varepsilon_F)$ is the half-width of the f levels, $\mathscr{E}_f$ is the energy of f levels measured from the Fermi energy ε_F, and $\gamma=V^2H(\varepsilon_F)$, where $H(\varepsilon_F)$ is the Hilbert transformation of $\rho(\varepsilon_F)$. Finally, the effective $\mathscr{J}$ value is

$$\mathscr{J}_{\rm eff}=\frac{V^2\mathscr{E}_f}{\Gamma^2+(\mathscr{E}_f+\gamma)^2} \ . \tag{2.20}$$

Comparing with the original formula $\mathscr{J}=|V|^2/\mathscr{E}_f$ obtained by the Schrieffer-Wolff transformation,[24] the direct scattering Hamiltonian (which gives rise to a phase shift of the band states and thus a finite linewidth of the f levels), yields a renormalized hybridization strength parameter $\mathscr{J}_{\rm eff}$. As the f levels move close to the Fermi energy, both $\mathscr{J}$ and Γ increase dramatically; but the increase of Γ tends to reduce $\mathscr{J}$, and the net effect yields an only slightly increased renormalized value $\mathscr{J}_{\rm eff}$. This effect is very important for the U^{3+} cases. Although the energy difference between the f levels and the Fermi energy for the U^{3+} ions ($\sim$0.5 eV) is much smaller than that for the Ce^{3+} ion ($\sim$2 eV), instead of a rapid increase in $\mathscr{J}$, we expect the effective value of $\mathscr{J}$ to be almost a constant as we move from Ce^{3+} to U^{3+}. This picture provides a basis for choosing the phenomenological input value of $\mathscr{J}$ in our theory. In Sec. IV C, we will discuss this further.

In our previous work,[5,8–10] the effect of the crystal field in splitting the levels of the ground-state multiplet of specified J (the total angular momentum of the ion) value has been shown to be one of the vital factors for understanding the main features of the magnetic behavior of moderately delocalized cerium and plutonium systems. (The other key factor is the strongly anisotropic two-ion interaction.) For these $J=\frac{5}{2}$ systems with cubic symmetry, the crystal-field Hamiltonian can be written as[30]

$$H_{\rm CF}=B_4(O_4^0+5O_4^4) \ , \tag{2.21}$$

where O_m^n are the Stevens operators.[30] The crystal-field splits the ground-state ionic multiplet into doublet Γ_7 and quartet Γ_8 states with crystal-field splitting $\Delta_{\rm CF}=360B_4$. If $B_4>0$, the ground state is a Γ_7 doublet; while the ground state is a Γ_8 quartet if $B_4<0$.

For the U^{3+} systems ($J=\frac{9}{2}$) with cubic symmetry, we follow the notation of Lea, Leask, and Wolf[31] and specify the crystal field through use of their parameters W and x. Then the crystal-field Hamiltonian is

$$H_{\rm CF}=W\left[x\frac{O_4^0+5O_4^4}{60}+(1-|x|)\frac{O_6^0-21O_6^4}{2520}\right] \ . \tag{2.22}$$

For $U^{3+}(5f^3)$, parameters W and x are related to V_4 and V_6 through the relations

$$V_4=-57.552Wx \ , \tag{2.23a}$$

$$V_6=-10.446W(1-|x|) \ . \tag{2.23b}$$

Since the experimental values of V_6 are much smaller than V_4, we neglect V_6 and take $x=1$ in our model calculations. Here V_4 and V_6 are related to the factors $B(4)$ and $B(6)$ defined in Ref. 31. They determine the scale of the crystal-field splitting and are linear functions of $\langle r^4\rangle$ and $\langle r^6\rangle$, respectively, the mean fourth and sixth powers of the radii of the magnetic electrons, and thus depend on the detailed nature of the magnetic ion wave functions. When $x=1$ and W is positive, the crystal-field states observed in order of increasing energy are a quartet $\Gamma_8^{(1)}$, a quartet $\Gamma_8^{(2)}$, and a doublet Γ_6; while when $x=1$ and $W<0$, the order becomes Γ_6, $\Gamma_8^{(2)}$, and $\Gamma_8^{(1)}$. The overall crystal-field splitting is about $0.8V_4$.

Summarizing the above discussion, our model Hamiltonian for a single ion at site i interacting via hybridization with the lattice of other ions can finally be written as

$$H_0=\sum_{\mathbf{k},M}\varepsilon_{\mathbf{k}}n_{\mathbf{k}M}+\sum_{M}\mathcal{E}_M n_M+\frac{U}{2}\sum_{MM'}n_M n_{M'}+H_{\mathrm{CF}}-\sum_{j}\sum_{MM'}\sum_{NN'}\mathcal{T}^{NN'}_{MM'}(\mathbf{R}_{ij})L^{(i)}_{M'M}L^{(j)}_{N'N}\ . \quad (2.24)$$

We solve the eigenvalue problem for H_0 in the mean-field (MF) theory, and the MF Hamiltonian is given by

$$(H_0)_{\mathrm{MF}}=\sum_i\sum_n \mathcal{E}^i_n L^{(i)}_{nn}\ , \quad (2.25)$$

where $\mathcal{E}_n$ denotes the energy of the MF state $|n\rangle$ on site i.

B. Equations-of-motion treatment of excitation behavior

To study the magnetic excitations we project the Fourier transformation of the Hamiltonian defined in Eq. (2.24) into the MF manifold. We treat the difference between the Hamiltonian H_0 of Eq. (2.24) and its mean-field approximation $(H_0)_{\mathrm{MF}}$ as a perturbation of the mean-field Hamiltonian. Using the random-phase-approximation (RPA) and the commutation relation[2]

$$[(H_0)_{\mathrm{MF}},L^{\mathbf{q}}_{nn'}]=(\mathcal{E}_{n'}-\mathcal{E}_n)L^{\mathbf{q}}_{nn'}\ , \quad (2.26)$$

and at low temperature considering only those transitions denoted by L_{n1} or L_{1n} where $\mathcal{E}_1$ is the mean-field ground-state energy, and $n\neq 1$ (appropriate transitions in the low-temperature regime), we have the equations of motion for the magnetic excitations[2]

$$[H_0-(H_0)_{\mathrm{MF}},L^{\mathbf{q}}_{nn'}]=2(\langle L^0_{nn}\rangle-\langle L^0_{n'n'}\rangle)\sum_{mm'}\mathcal{T}^{mm'}_{n'n}L^{\mathbf{q}}_{mm'}\ . \quad (2.27)$$

The thermal average $\langle L^0_{nn}\rangle$ is unity if n is the ground state ($n=1$) and zero otherwise. The dynamical matrix is a 10×10 matrix, including upward and downward transitions between the ground state and each of the five excited states for a $J=\frac{5}{2}$ system, such as $Ce^{3+}(4f^1)$ and $Pu^{3+}(5f^5)$. For $U^{3+}(5f^3)$ systems, $J=\frac{9}{2}$, there are nine excited states, and hence the matrix is 18×18. On diagonalizing the dynamical matrix we obtain the magnetic excitation modes. For these RPA modes, the calculation of the intensities is straightforward (see Ref. 2 for the details). The more intense modes along the (001) and (100) directions are indicated by the more heavily drawn parts of the dispersion curves shown in Figs. 1 and 2. (The boldly drawn parts of the curves indicate modes with intensity differing by at most a factor of 4 from the most intense mode.)

III. RELAXATION EFFECTS ON EXCITATIONS

To understand the unusual spectrum observed by the neutron inelastic scattering we calculate the imaginary part of the dynamic susceptibility $\mathrm{Im}\chi(\mathbf{q},\omega)$ [or $\chi''(\mathbf{q},\omega)$] which is proportional to the correlation function $S(\mathbf{q},\omega)$ and hence proportional to the differential neutron-scattering cross section via

$$\frac{d^2\sigma}{d\Omega\, d\omega}\sim S(\mathbf{q},\omega)\sim\frac{1}{1-e^{-\beta\omega}}\,\mathrm{Im}\chi(\mathbf{q},\omega)\ , \quad (3.1)$$

where $\beta=1/k_BT$. In this section we use the projection-operator method developed by Mori *et al.*[21] to derive the formalism for obtaining the dynamic susceptibility.

Generally, a susceptibility can be written as[21,32,33]

$$\chi_{AB}(z)=i\int_0^\infty dt\, e^{izt}\langle[A^\dagger,B(-t)]\rangle=\left\langle\left[A^\dagger,\frac{1}{\mathcal{L}-z}B\right]\right\rangle\ , \quad (3.2)$$

where A and B are the dynamic variables, and $\mathcal{L}$ is a Liouville operator defined by

$$\mathcal{L}A(t)\equiv i[H,A(t)]\ . \quad (3.3)$$

Since

$$\langle[A^\dagger,B]\rangle=\int_0^\beta d\lambda\langle A^\dagger e^{-\lambda\mathcal{L}}\mathcal{L}B\rangle=\beta\langle A|\mathcal{L}|B\rangle\ , \quad (3.4)$$

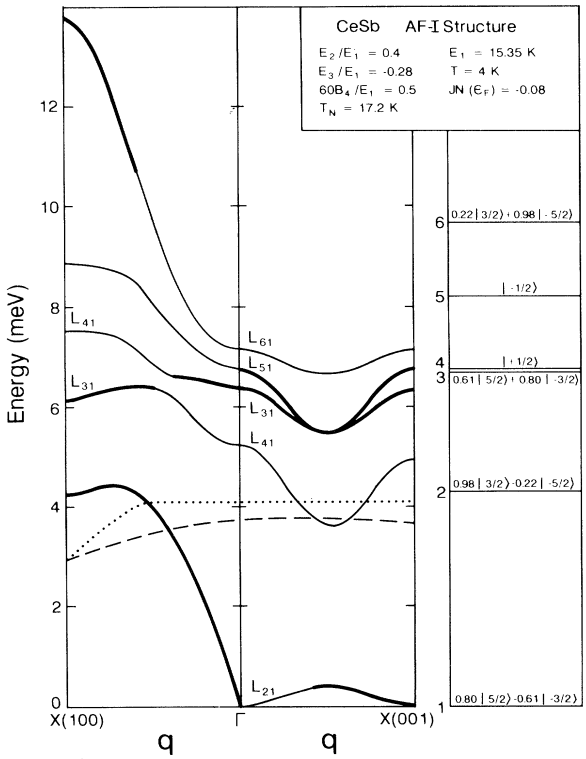

FIG. 1. Calculated dispersion curves for excitations in the AF-I phase of CeSb at $T=4$ K with $E_2=0.4E_1$, $E_3=-0.28E_1$, and $60B_4=0.5E_1$ for $\mathbf{q}$ along [001] and [100] (directions parallel and perpendicular to the moment direction, respectively). $E_1=15.35$ K to match experimental $T_N=16.2$ K. The solid curves show the behavior calculated in the random-phase approximation (RPA). The heavily drawn solid curves show the intense modes expected to be observed in the RPA. The energy levels of the molecular-field states and their compositions in terms of the angular momentum eigenstates (quantized along [001]) are shown on the far right. The dashed curve is the calculated dispersion curve after including the damping and shift effects with $\mathcal{J}N(\varepsilon_F)=-0.08$. The dotted curve shows the experimental results of Rossat-Mignod *et al.* (Ref. 12) at $T=4$ K for CeSb.

we have

$$\chi_{AB}(z)=\beta\left\langle A\left|\frac{\mathcal{L}}{\mathcal{L}-z}\right|B\right\rangle , \tag{3.5}$$

$$\chi_{AB}(0)=\beta\langle A|B\rangle , \tag{3.6}$$

and

$$\frac{1}{z}[\chi_{AB}(z)-\chi AB(0)]=-\beta\left\langle A\left|\frac{1}{z-\mathcal{L}}\right|B\right\rangle =-\beta C_{AB}(z) . \tag{3.7}$$

Here $C_{AB}(z)$ is an autocorrelation function defined as

$$C_{AB}(z)=\left\langle A(0)\left|\frac{1}{z-\mathcal{L}}\right|B(0)\right\rangle =\int_0^\infty dt\, e^{-izt}\langle A(0)e^{-i\mathcal{L}t}B(0)\rangle . \tag{3.8}$$

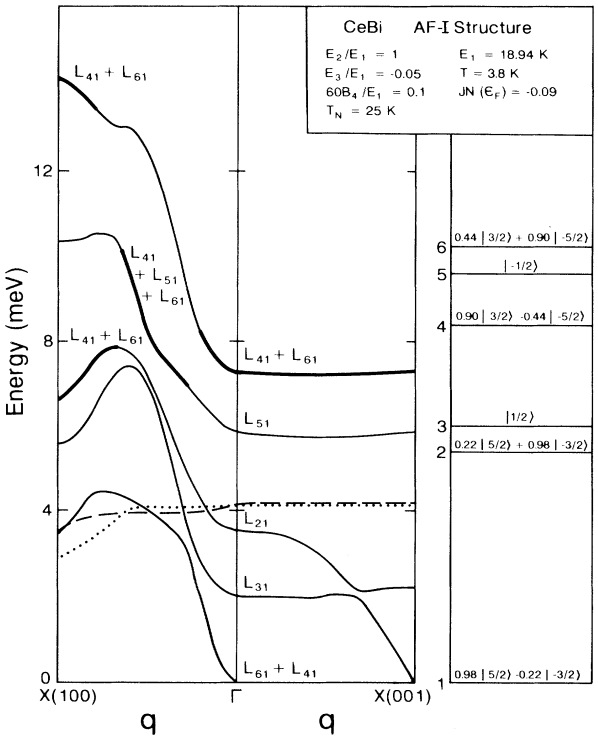

FIG. 2. Calculated dispersion curves for excitations in the AF-I phase of CeBi at $T=3.8$ K, with $E_2=E_1$, $E_3=-0.05E_1$, and $60B_4=0.1E_1$ for $\mathbf{q}$ along the [001] and [100] directions. $E_1=18.94$ K to fit the experimental $T_N=25$ K. The solid curves show the behavior calculated in the random-phase approximation (RPA). The heavily drawn parts of these curves show the intense modes expected to be observed in the RPA. The dashed curve shows the calculated result after including the relaxation effect with $\delta N(\varepsilon_F)=-0.09$. The dotted curve shows the experimental results of Rossat-Mignod *et al.* (Ref. 12) at $T=4$ K for CeBi. The energy levels of the molecular-field states and their compositions in terms of the angular momentum eigenstates are shown on the far right.

Next we introduce the projection operator[21]

$$Q\equiv 1-|A\rangle\langle A|A\rangle^{-1}\langle A|\equiv 1-P . \tag{3.9}$$

If we use the expansion relation

$$\frac{1}{z-\mathcal{L}Q}=\frac{1}{z}\left[1+\frac{1}{z}\mathcal{L}Q+\frac{1}{z^2}\mathcal{L}Q\mathcal{L}Q+\cdots\right] , \tag{3.10}$$

and the algebraic operator identity

$$\frac{1}{x-y}=\frac{1}{x}\left[1+\frac{y}{x-y}\right] , \tag{3.11}$$

we obtain

$$C_{AB}(z)=\frac{1}{z-\Omega-\Sigma}C_{AB}(0) , \tag{3.12}$$

where

$$\Omega=\frac{1}{C_{AB}(0)}\langle A|\mathcal{L}|A\rangle , \tag{3.13}$$

and

$$\Sigma=\left\langle \dot{A}\left|Q\frac{1}{z-Q\mathcal{L}Q}Q\right|\dot{A}\right\rangle C_{AB}^{-1}(0) . \tag{3.14}$$

$\Sigma(z)$ is the Laplace transform of the memory function[21] and $\dot{A}=dA/dt$. To obtain Eq. (3.14) we have used

$$\mathcal{L}=\mathcal{L}(P+Q) , \tag{3.15}$$

$$P|A\rangle=|A\rangle , \tag{3.16a}$$

$$Q|A\rangle=0 . \tag{3.16b}$$

This provides the needed formalism, and we now return to the problem at hand. What we need is the magnetic dynamic susceptibility. If we write the angular momentum operator J as

$$J=\sum_{m,n}J_{mn}L_{mn} , \tag{3.17}$$

with $J_{mn}=\langle m|J|n\rangle$ and $L_{mn}=|m\rangle\langle n|$, then according to Eq. (3.5) the single-ion magnetic susceptibility $\chi(z)$ can be rewritten as

$$\chi(z)=\beta\sum_{mn}\sum_{m'n'}J_{mn}J_{m'n'}\left\langle L_{nm}\left|\frac{\mathcal{L}}{\mathcal{L}-z}\right|L_{m'n'}\right\rangle \tag{3.18}$$

or

$$\frac{1}{z}[\chi(z)-\chi(0)]=\beta\sum_{mn}\sum_{m'n'}J_{nm}J_{m'n'}C_{mn,m'n'}(z) , \tag{3.19}$$

with the autocorrelation function

$$C_{mn,m'n'}(z)=\left\langle L_{nm}\left|\frac{i}{z-\mathcal{L}}\right\}L_{m'n'}\right\rangle =\frac{1}{z-(\mathcal{E}_{m'}-\mathcal{E}_{n'})-\Omega_{mn,m'n'}-\Sigma_{mn,m'n'}}\times C_{mn,m'n'}(0) , \tag{3.20}$$

where

$$\Omega_{mn,m'n'}=\langle L_{mn}|\mathcal{L}'|L_{m'n'}\rangle C^{-1}_{mn,m'n'}(0)$$
$$=i\langle \dot{L}_{nm}|L_{m'n'}\rangle C^{-1}_{mn,m'n'}(0)\ , \tag{3.21}$$

$$\Sigma_{mn,m'n'}=\left\langle \dot{L}_{mn}\left|Q\frac{1}{z-Q\mathcal{L}Q}Q\right|\dot{L}_{m'n'}\right\rangle C^{-1}_{mn,m'n'}(0)\ , \tag{3.22}$$

$$C_{mn,m'n'}(0)=\langle L_{nm}|L_{m'n'}\rangle\ . \tag{3.23}$$

Treating the single-ion hybridization exchange scattering interaction $H_{\rm ex}$ given by Eq. (2.9) as the main relaxation mechanism for the damping and the line shifts of the magnetic excitations our Hamiltonian is

$$H=H_0+H_{\rm ex}\ . \tag{3.24}$$

We characterize H_0 of Eq. (2.24) by the excitation energy gaps $\mathscr{E}_m$ and excitation transition operators L_{mn}. Here m,n denote the ground state and five excitation states for Ce^{3+} and Pu^{3+} systems, and nine excitation states for U^{3+} systems.

We expand $1/(z-Q\mathcal{L}Q)$ in Eq. (3.22) as a power series in $Q\mathcal{L}Q$ and use the relations[33]

$$P|\dot{A}\rangle=0\ , \tag{3.25a}$$
$$Q|\dot{A}\rangle=|\dot{A}\rangle\ , \tag{3.25b}$$
$$Q\mathcal{L}^n|\dot{A}\rangle=\mathcal{L}^n|\dot{A}\rangle\ , \tag{3.26}$$

and the general commutation rules[33]

$$[L_{mn},L_{m'n'}]_{\pm}=L_{mn'}\delta_{nm'}\pm L_{m'n}\delta_{mn'}\ . \tag{3.27}$$

Then the line broadening is given by $\frac{1}{2}\,\mathrm{Im}\Sigma_{mn,m'n'}$ and the line shift is $\Omega_{mn,m'n'}+\mathrm{Re}\Sigma_{mn,m'n'}$. We have calculated Ω, and for the systems we have investigated the contribution of Ω to the shift is small and is therefore neglected. The calculation of Σ is straightforward. Up to order of $\mathscr{J}^2$ we have

$$\Sigma_{mn,m'n'}(\omega)=\frac{T}{\omega}\left[2F_{mn}(\omega)+\sum_l\left[F_{ml}(\omega)+F_{ln}(\omega)\right]\right]$$
$$\times C^{-1}_{mn,m'n'}(0)\delta_{mm'}\delta_{nn'}\ , \tag{3.28}$$

with

$$C_{mm,mm}=p_m\ , \tag{3.29}$$

$$C_{mn,m'n'}(0)=-\delta_{mm'}\delta_{nn'}T\left[\frac{p_n-p_m}{\mathscr{E}_n-\mathscr{E}_m}\right]\ , \tag{3.30}$$

$$\mathrm{Re}F_{mn}(\omega)=2[\mathscr{J}N(\varepsilon_F)]^2\left\{(p_n-p_m)\omega\ln\left[\frac{D}{2\pi T}\right]-(p_n-p_m)\omega\,\mathrm{Re}\Psi\left[1-i\frac{\omega-\mathscr{E}_m+\mathscr{E}_n}{2\pi T}\right]\right.$$
$$\left.+(p_n-p_m)(\mathscr{E}-\mathscr{E}_n)\left[\mathrm{Re}\Psi\left[1-i\frac{\omega-\mathscr{E}_m+\mathscr{E}_n}{2\pi T}\right]-\mathrm{Re}\Psi\left[1-i\frac{\mathscr{E}_n-\mathscr{E}_m}{2\pi T}\right]\right]\right\}\ , \tag{3.31}$$

$$\mathrm{Im}F_{mn}(\omega)=2\pi p_n[\mathscr{J}N(\varepsilon_F)]^2(\omega-\mathscr{E}_m+\mathscr{E}_n)\frac{1-e^{-\beta\omega}}{1-e^{-\beta(\omega-\mathscr{E}_m+\mathscr{E}_n)}}\ . \tag{3.32}$$

Here p_n are the thermal occupation numbers of the states $|n\rangle$, D is the cutoff energy of the band [see discussion preceding Eq. (2.9)], and Ψ is the digamma function defined as

$$\Psi(z)=\int_0^\infty dt\left[\frac{e^{-t}}{t}-\frac{e^{-tz}}{1-e^{-t}}\right],\quad \mathrm{Re}z>0\ . \tag{3.33}$$

IV. RESULTS AND DISCUSSION

In this section we apply the theory to Ce^{3+}, Pu^{3+}, and U^{3+} systems. We attack the problem of finding the excitation damping effects sequentially. We first solve the eigenvalue problem for H_0 of Eq. (2.24) in the mean-field theory, $(H_0)_{\rm MF}$ [Eq. (2.25)], to obtain a $(2J+1)$ energy-level structure including effects of the hybridization-mediated two-ion interactions and the crystal-field effects. We phenomenologically choose the set of range parameters E_1,E_2,E_3 and the crystal-field parameter B_4 to fit the observed equilibrium magnetic properties (such as phase diagrams, transition temperatures, magnetic moments) and the crystal-field splittings. The second step is to solve the equation of motion, Eq. (2.27), in the mean-field representation for $H_0-(H_0)_{\rm MF}$ to obtain the magnetic-excitation dispersions in the random-phase approximation (RPA). Then the imaginary part of the dynamic susceptibility can be obtained from Eqs. (3.19), (3.20), and (3.28)–(3.32). In this step only one adjustable parameter $\mathscr{J}N(\varepsilon_F)$, the product of the single-site hybridization strength and the band density of states at the Fermi energy, is introduced.

A. Application to CeBi and CeSb

Among cerium compounds, the rocksalt structure monopnictides and monochalcogenides of cerium provide a class of anomalous compounds with highly unusual magnetic properties. In particular, the heavier monopnictides, CeSb and CeBi, are characterized by a very large magnetic anisotropy favoring alignment along the cube-edge direction of the NaCl lattice,[35,36] a large reduction[34] of the crystal-field splitting from the value expected

from extrapolation from the heavier rare-earth monopnictides, a complex magnetic phase diagram containing unusual magnetic structures,[37–39] and unusual magnetic excitation spectra.[11,12] These anomalous features of the cerium monopnictides are distinct from those often found in other cerium compounds in which strong f-d-electron interactions give rise to "Kondo-like" (f-moment screening) behavior.[40]

CeSb exhibits the most complex phase diagram, containing at least 14 different magnetic structures for external field $H<70$ kOe.[38–40] It orders with a first-order transition at[40] $T_N \simeq 16.2$ K and undergoes six additional first-order phase transitions in zero field.[40] The high-temperature phases (>8.5 K) (referred to as AFP) are commensurate with the lattice and correspond to a periodic stacking of nonmagnetically ordered (P) and ferromagnetic (001) planes with an up and down magnetization along a [001] direction and a moment that is close to saturation ($\sim 2.1\mu_B$).[38,39] In zero field, the nonmagnetic planes are isolated, i.e., they always have neighboring up and down ferromagnetic planes, and the distance between the P layers increases with decreasing temperature. Below 8.5 K the nonmagnetic planes disappear, giving a type-IA antiferromagnetic structure ($++--$). On the other hand, CeBi has simpler, though still unusual, magnetic structure behavior.[2,41] It orders in a type-I ($+-$) antiferromagnetic phase at 25 K and undergoes a transition to a type-IA antiferromagnetic structure at about 12.5 K. The direction and magnitude of equilibrium moments are as in CeSb. The equilibrium properties of CeSb and CeBi are summarized in Table I.

Additional unusual behavior is seen in the crystal-field measurements.[34] For both CeBi and CeSb the observed magnitudes of the crystal-field splitting are much smaller than the extrapolated values from other rare-earth monopnictides. The expected[34] magnitude of crystal-field splitting between Γ_7 and Γ_8 should be 247 K for CeBi and 264 K for CeSb, while the observed[43] values are about 8 and 37 K, respectively. As we have pointed out in Sec. II, this behavior can be understood[6] by the hybridization dressing effect.

The large cube-edge anisotropy[35,36] and complex phase diagrams[40] found in CeSb were successfully explained[1,2,6,7] on the basis of the hybridization-mediated two-ion interaction acting along with the cubic crystal-field interaction using the theory discussed in Sec. II. It was found that upon choosing[7] the range parameters $E_1=15.35$ K, $E_2=0.4E_1$, $E_3=-0.28E_1$, and the crystal-field splitting parameter $60B_4=0.5E_1$ ($\Delta_{CF}=45$ K), that the high-temperature AFP structure can be stabilized, and it undergoes a phase transition to a type-IA antiferromagnetic structure at about 8.5 K.

Beside the unusual equilibrium behaviors some very interesting dynamic features have been observed in CeSb and CeBi in neutron-inelastic-scattering experiments. For neutron-inelastic-scattering studies on polycrystalline samples, Heer *et al.*[11] reported that there is only one well-separated inelastic peak observed for both CeSb and CeBi. At low temperature (<4 K), the position of the peak is 5.2 meV for CeBi and 4.1 meV for CeSb; and the full linewidth at the half maximum of the peak energy is 1.2 meV for CeBi and 1.0 meV for CeSb. Later Rossat-Mignod *et al.*[12] reported that for both CeBi and CeSb the energy gap in the magnetic excitation spectrum at $\mathbf{q}=(000)$ is $4.1\pm$ meV, the linewidth is less than 1 meV, and the spectrum is almost dispersionless across the whole Brillouin zone except near the zone boundary at $\mathbf{q}=(100)$ where the energy minimum occurs. This close similarity for CeBi and CeSb found in Ref. 12 is quite surprising because the crystal-field splitting and the ordering temperature are quite different.

Our theory can satisfactorily explain this puzzling problem. The spectra observed by Rossat-Mignod[12] (shown by the dotted curves) and the calculated results at low temperature for CeSb and for CeBi are shown in Figs. 1 and 2, respectively. The energy levels of the mean-field states and their compositions in terms of the angular momentum eigenstates (quantized along [001]) are shown on the far right in the figures. The six mean-field energy-level states are no longer the pure crystal-field doublet Γ_7 and quartet Γ_8 states, but are a mixture of these because of the strong two-ion interactions. To determine the values of the range parameters E_1, E_2, E_3 and the hybridization dressed crystal-field parameter B_4 for CeSb, following Kioussis *et al.*[7] we choose the ratios $E_2/E_1=0.4$, $E_3/E_1=-0.28$, and $60B_4/E_1=0.5$ to stabilize the correct antiferromagnetic AFP phase in the temperature range $8.5<T<16.2$ K and the type-IA structure below 8.5 K, and the value of $E_1=15.35$ K to fit the experimental $T_N=16.2$ K. (For this E_1, $\Delta_{CF}=360B_4\simeq 45$ K, is quite close to the observed value of 37 K.) While for CeBi, the ratios are $E_2/E_1=1$, $E_3/E_1=-0.05$ to stabilize AF-I and AF-IA antiferromagnetic phase above and below 12.5 K, respectively, $E_1=18.94$ K to fit the experimental $T_N=25$ K, and $60B_4/E_1=0.1$ to fit the observed crystal-field splitting $\Delta_{CF}\sim 8$ K.

Using the mean-field states as a basis we calculate the magnetic excitation dispersions by solving the RPA equation of motion, Eq. (2.27). The calculated dispersion curves for excitations in the AF-I antiferromagnetic phase at low temperature are shown in Figs. 1 and 2 by the solid curves for CeSb and CeBi, respectively. (To simplify the calculations, the AF-I phase is used instead of the AF-IA phase at low temperature. While the IA structure by reducing the Brillouin zone allows some additional band splittings, in practice,[26(b)] these are small and would be expected to have negligible effect on the way in which the band structure affects the relaxation.) For CeSb, for $\mathbf{q}$ along the [001] ordered-moment direction the dominant modes in intensity, which are expected to be observed in experiments, are L_{31} and L_{51}, which have an excitation energy minimum (~ 5.5 meV) at $q=0.5$ and maximum (~ 7.5 meV) at both the Γ point and the zone boundary (L_{21} has significant intensity but a very low energy, and it might be difficult to be distinguished from the experimental peak around zero energy transfer); while along the [100] direction the energies of the most intense modes L_{21}, L_{31}, and L_{61} are strongly $\mathbf{q}$ dependent. (We note that for CeSb, because we have adopted the range and crystal-field parameters of Ref. 7,

designed to reproduce the unusual magnetic structural behavior in the appropriate temperature ranges, the ordered moment at low temperature differs significantly from the experimental near-saturation value.) For CeBi, a most intense mode, which is a mixture of L_{41} and L_{61} modes, with a flat excitation dispersion with energy gap ~ 7.2 meV through the whole zone from the Γ point to the zone boundary is obtained for $\mathbf{q}$ along the [001] direction. And, as in CeSb, along [100] we obtained the mode intensity sharing effect and the strongly $\mathbf{q}$-dependent energies.

The extreme discrepancy between the predicted RPA (heavy solid curves in the figures) and the observed[12] (dotted curves) magnetic excitation dispersion curves for CeSb and CeBi can be removed if we include in our calculations the strong renormalization of the magnetic excitations caused by the hybridization-induced relaxation. The damping and shifts of the magnetic excitations result in completely different spectra from the RPA results. The dashed curves in Figs. 1 and 2 are our calculated dispersion spectra after the relaxation is taken into account at low temperature for CeSb and CeBi, respectively. They exhibit the following behavior: the excitation energy transfer is ~ 4.1 meV for CeBi and ~ 3.7 meV for CeSb at the Γ point, and there is a flat dispersion curve across most of the Brillouin zone except near the zone boundary at $\mathbf{q}=(100)$ where the energy minimum occurs. Along (001) this flat curve is the result of the correlated combination between the RPA L_{31} and L_{51} modes, while along (100) it is the result of the correlated combination between L_{31}, L_{51}, and L_{21}. The most striking fact is that the predicted spectrum for CeSb is almost identical with the predicted spectrum for CeBi except that the excitation energy is slightly smaller for CeSb (~ 3.7 meV compared with the observed[12] ~ 4.1 meV). In this step of the calculations the only adjustable parameter is $\mathcal{J}N(\varepsilon_F)$. We choose its values to fit the experimental linewidths at the Brillouin zone center. Since the observed linewidths are[11] about 1 meV for both CeSb and CeBi, and the experimental resolutions are also about 1 meV, it is difficult to determine what the real line-widths are. We choose $\mathcal{J}N(\varepsilon_F)\sim -0.08$ for CeSb and ~ -0.09 for CeBi (compared to the first-principles calculated value of -0.07 by Wills and Cooper[6] for both CeSb and CeBi) to fit the linewidths of 1 meV at the Γ point. From Eqs. (3.28), (3.31), and (3.32), the linewidth and the line shift from RPA go quadratically as $\mathcal{J}N(\varepsilon_F)$. Thus, for example, in CeSb changing $\mathcal{J}N(\varepsilon_F)$ from -0.08 to -0.06 (as compared to the first-principles calculated value of -0.07) would cut the linewidth and line shift almost in half, i.e., reduces the linewidth at Γ from about 1 meV to about 0.5 or 0.6 meV.

Note that the values of range parameters E_1, E_2, E_3, and crystal-field parameter B_4 determined by previous[7] static calculations are kept unchanged when we calculate the damping and shifts of the magnetic-excitation spectra. It is quite impressive that by using only one adjustable parameter $\mathcal{J}N(\varepsilon_F)$ (to fit the experimental linewidths at the Brillouin zone center only) our theory fully explains the very unusual similarity of the anisotropic magnetic excitation behaviors for CeSb and CeBi observed by Rossat-Mignod.[12] Because we use the same set of parameters in the calculations to obtain both correct static and correct dynamic behaviors at the same time, some small sacrifice must be made. For CeSb, to obtain both the complex phase diagram and the correct dispersion at the same time, the calculated magnitude of the intense mode energy is not quite as good in overall comparison to experiment as that obtained for CeBi which has a much simpler phase diagram; and as noted above, for CeSb the ordered moment at low temperature differs significantly from the experimental near-saturation value.

B. Application to PuSb

Among plutonium monopnictides with the rocksalt structure PuSb is the one which has been best studied both experimentally[19,20] and theoretically.[2,5,42] PuSb shows magnetic structures with strong [001] anisotropy. It orders in a longitudinal polarized (modulation wave vector parallel to the moment direction) long-period antiferromagnetic below the $T_N=85$ K and undergoes a first-order transition to a [001] ferromagnet at $T=67$ K. At 10 K in the ferromagnetic phase, the ordered f moment is $(0.76\pm 0.03)\mu_B$, and an almost dispersionless magnetic transition with an energy of 4.3 THz was observed in the neutron-inelastic-scattering studies on a single domain crystal.[20] At the zone boundary for the wave vector $\mathbf{q}=(100)$ (transverse to the magnetization) there exist two excitations: the mode at 4.3 THz polarizes along the [010] direction (transverse to both the magnetization and the wave vector), whereas the mode at 3.5 THz has polarization along the wave vector ([100] direction). At (0.7,0,0) two separate modes can no longer be distinguished.

In previous theoretical studies,[2,5,42] by transforming the band-f hybridization into a band-f resonant scattering from the correlated multiplet states of the plutonium ions, and considering only the scattering processes that involve f electrons in the $m_l=0$, $m_s=\pm\frac{1}{2}$ states (for quantization along the interionic axis) which dominate the two-ion interactions, the major features of the unusual static magnetic behavior of PuSb have been understood. The large magnetic anisotropy and the main features of the unusual magnetic phase diagram were explained[2,42] in the mean-field framework. However, the correct longitudinally polarized antiferromagnetic phase could be satisfactorily obtained[5] only by considering the contribution of additional scattering channels (single-site scattering processes involving f electrons with $m_l=\pm 1$, $m_s=\mp\frac{1}{2}$). The magnetic excitation spectrum as obtained in the RPA by solving the equations of motion [see Eq. (2.27)] showed remarkable agreement with the unusual experimental behavior with one important discrepancy. This is that we predict that the major mode intensity across the Brillouin zone is not in the largely dispersionless mode (and hence also our lower-energy mode at the zone boundary does not occur at an energy minimum). (See Fig. 6 of Ref. 5. The discrepancy is that across most of the zone, the theoretically predicted intensity is concentrated in the mode labeled L_{41} rather than in that labeled L_{31}. Note that in the figure caption, $\mathbf{q}$ along [100]

is mislabeled as being parallel, rather than perpendicular to the moment direction.)

Now we apply the relaxation theory to PuSb to see what happens. Using the same values of the range parameters $E_1=121$ K, $E_2/E_1=1$, $E_3/E_1=-0.306$, and the crystal-field parameter $60B_4/E_1=-0.38$ used in earlier work,[5] we have calculated the imaginary part of the dynamic susceptibility vs frequency. We find that (1) the relaxation effect shifts the magnetic-excitation spectrum somewhat toward lower energies across the whole Brillouin zone for $\mathbf{q}$ in both the [001] and the [100] directions; (2) for values of $\mathcal{J}N(\varepsilon_F)$ in the range $-0.06--0.10$ the damping effect changes neither the shape of the dispersion curve nor the polarization of the modes. This leaves unresolved the remaining discrepancy between theory and experiment for the PuSb behavior, the intensity distribution between the modes labeled L_{31} and L_{41} in Fig. 6 of Ref. 5. Presumably, the present treatment of the subtleties of the $5f^5$ Pu^{3+} intraionic coupling (intraionic correlation effects) is adequate[5] to capture the correct polarization of the magnetic structure, but is not sufficient to capture the mode intensity distribution. We note that a large negative value of $\mathcal{J}N(\varepsilon_F)$ (<-0.09) eliminates having two branches at the zone boundary with $\mathbf{q}$ along [100] (transverse to moment) direction. Hence the appropriate value of $\mathcal{J}N(\varepsilon_F)$ should be less negative than -0.09, and we chose it to be -0.08 to fit the correct linewidth of ~ 0.5 THz at the Γ point.

It is interesting to notice that contrary to the Ce^{3+} cases, in which the damping and shift effects dramatically change the dispersion, for PuSb the damping of the excitations does little to change the spectrum; and, on the other hand, the value of range parameter $E_1=121$ K is about six times larger than in the cerium cases ($E_1\sim 20$ K) despite the value of $\mathcal{J}N(\varepsilon_F)$ being the same for both systems. The lack of change in the value of $\mathcal{J}N(\varepsilon_F)$ is reasonable because for PuSb the magnitude of $\mathcal{E}_f$, the energy difference between the f levels and the Fermi energy, is almost equal to that in the Ce^{3+} systems (~ 2 eV). Hence, the strength of the band-f hybridization is of the same order. The question is how to explain the fact that for PuSb there is a large increase in the two-ion interactions (characterized by E_1) when the single-ion hybridization strength $\mathcal{J}$ does not increase from the Ce^{3+} cases. We believe that the large increase in E_1 is from the band-structure difference between the Pu^{3+} and Ce^{3+} systems with regard to the f-f overlap, and we will discuss this matter below in Sec. IV C.

C. Application to UAs, UP, and UTe

The uranium monopnictide and monochalcogenide compounds, which form in NaCl structure, show a great variety of interesting magnetic properties associated with the behavior of the $5f$ electrons in these materials.[14–18] In particular, the pnictides order antiferromagnetically with a variety of magnetic structures and transitions, while the chalcogenides order ferromagnetically. USb orders in a 3-$\mathbf{k}$ type-I structure below T_N of 214 K, UAs orders at about 125 K in a single-$\mathbf{k}$ type-I structure and undergoes a phase transition to a 2-$\mathbf{k}$ type-IA structure at about 66 K with an ordered magnetic moment $\sim 2.24\mu_B$ at low temperature, UP also orders in a single-$\mathbf{k}$ type-I structure at $T_N=125$ K and goes to a 2-$\mathbf{k}$ type-I structure at about 23 K with an ordered moment $\sim 1.9\mu_B$, UTe is in a ferromagnetic structure at all temperatures below $T_c=104$ K and at 5 K exhibits a magnetic moment of $2.25\mu_B$ with the easy direction being $\langle 111\rangle$. The static magnetic properties are summarized in Table I. Despite the well-defined magnetic ordering, clearly defined magnetic excitation lines, as might be expected, are not observed in neutron-inelastic-scattering experiments on these systems except for USb and UTe which have larger lattice parameters. Instead there appears to be a continuous spectrum of magnetic response.[14] Even when clearly defined collective magnetic excitations are observed as in USb and UTe, these are imposed on a broad continuum, and the clearly defined excitations tend to disappear well below the transition temperatures. Detailed information for UTe is available through neutron-inelastic-scattering experiments performed by Lander *et al.*[18] on a single domain crystal of ferromagnetic UTe. They observed very large anisotropy of both the dispersion relations and the damping of the excitations. The excitation transition energy at Γ is about 3.6 THz, and the full linewidth at half maximum is ~ 0.5 THz; along the $[qqq]$ direction the energy rises to 8.8 THz, and the linewidth increases to 1 THz at the zone boundary $q=0.5$; in the $[q\bar{q}0]$ direction the excitation starts with the same dispersion as along the $[qqq]$ direction, but by $q=0.25$ the dispersion is much reduced, and the curve is essentially flat at ~ 5.3 THz for $0.35<q<0.55$. Along this direction the broadening increases rapidly. The linewidth is greater than 2 THz at $q=0.4$, and the magnetic response peak cannot be observed for $q>0.55$.

Although intensively studied in the past ten years, the unusual magnetic properties discussed above are still far from completely understood. Because, in contrast to their $4f$ counterpart in cerium, the wave functions of the $5f$ electrons in uranium are spatially much more extended and the corresponding states are energetically less stable (f electrons are more itinerant), a site-based approach is not of general validity. On the other hand, the band-based itinerant approach is probably too extreme in the opposite direction. Uranium compounds thus stand at the interface of localized and itinerant magnetism. Our theory, a site-based approach, is strongly renormalized by the hybridization-mediated two-ion interactions, the hybridization dressed crystal-field interaction, and the hybridization-induced relaxation. In this section we apply our theory to $U^{3+}(5f^3)$ systems. Among the compounds with small lattice parameters we choose UAs and UP as examples, while in the compounds with the larger lattice parameters, we choose UTe to test our theory. The results show that our theory is appropriate for describing the unusual magnetic behaviors observed in uranium monopnictides and monochalcogenides.

Since the Coulomb integral U of ~ 3 eV is much larger than the energy difference between the f levels and Fermi energy (~ 0.5 eV), we neglect the fluctuations between different configurations and assume $5f^3$ as the stable configuration for U^{3+}. Because of the large spin-orbit in-

teraction which gives a $J=\frac{9}{2}$ ground state, $^4I_{9/2}$ is taken to be the quasi-ion ground state. The crystal field splits this into a doublet Γ_6, a quartet $\Gamma_8^{(1)}$, and a quartet $\Gamma_8^{(2)}$ states. We then carry out the mean-field calculations including both hybridization-mediated two-ion interactions and the hybridization dressed crystal-field splitting and obtain the mean-field states and energy levels. The strong two-ion interactions remove the degeneracy in the crystal-field Γ_6 doublet and $\Gamma_8^{(1)}$ and $\Gamma_8^{(2)}$ quartet states, and this results in 10 system energy-level states. For UAs and UP, the range parameters E_1, E_2, E_3 are determined by the following criteria:[9] (1) choosing the ratios E_2/E_1 and E_3/E_1 to stabilize the correct antiferromagnetic phase at low temperature, and (2) choosing the value of E_1 to match the experimental T_N, while the values of crystal-field parameters W and x are chosen to obtain the correct magnetic moments at low temperature. For UAs, we choose $E_2/E_1=1$, $E_3/E_1=-0.5$ to obtain the AF-I phase and $E_1=500$ K to fit $T_N=127$ K; the values of W and x are chosen to be $-0.02E_1$ and 1 ($\Delta_{CF}=460$ K) to give the observed moment $2.0\mu_B$; and for UP, the ratios are $E_2/E_1=1$, $E_3/E_1=-0.6$ to stabilize the AF-I phase and $E_1=215.5$ K to match the experimental $T_N=125$ K, $W=-0.05E_1$, and $x=1$ ($\Delta_{CF}=496$ K) to obtain the moment $\sim 2.1\mu_B$. Notice that the easy direction is $\langle 100\rangle$ for UP and $\langle 001\rangle$ for UAs (where the single-k structure propagates along $\langle 001\rangle$). When we calculate the resonant scattering coefficient $A_{mm'}^{MM'}$ in Eq. (2.15) the additional scattering channels ($m=\pm\frac{1}{2}$, $m_l=\pm 1$, $m_s=\mp\frac{1}{2}$) have to be included beyond the dominant scattering channel ($m=\pm\frac{1}{2}$, $m_l=0$, $m_s=\pm\frac{1}{2}$) to obtain the correct polarization for UAs as we did[5] in the case of PuSb. For UTe, we choose the ratios $E_2/E_1=1$, $E_3/E_1=-0.5$ to stabilize the ferromagnetic phase in the entire temperature range below $T_c=104$ K, $E_1=150$ K to fit observed T_c, $W=0.005E_1$ and $x=1$ ($\Delta_{CF}=34.5$ K) to give the moment $\sim 2.6\mu_B$.

In the mean-field representation at low temperature we calculate the dispersion and then the damping of the magnetic excitations for the AF-I structure with moments periodically stacked along [001] in UP and UAs, and for the ferromagnetic structure with the easy direction along [111] in UTe. Figures 3–5 show the imaginary part of the dynamic susceptibility $\chi''(\omega)$ vs frequency $\hbar\omega$ for UAs, UP, and UTe, respectively. Beside the parameters E_1, E_2, E_3, W, and x, which remained unchanged from their values used in the mean-field calculations, we also use a parameter $\delta N(\varepsilon_F)$. Its values are chosen to be -0.11 for UP, -0.12 for UAs, and -0.09 for UTe.

As can be seen in Fig. 3 for UAs, at $T=11$ K, broad continuous responses are obtained at both the zone center and at the boundary $\mathbf{q}=(001)$; while a very broad excitation is distinguishable at $\mathbf{q}=(100)$. For UP, Fig. 4 shows that at $T=4.2$ K a very broad excitation can be identified at the Γ point with a full linewidth at half maximum of ~ 5 THz, but a continuous spectrum is obtained at $\mathbf{q}=(001)$ and (100).

The most interesting results are obtained for UTe (shown for specific $\mathbf{q}$ values in Fig. 5, and with the calcu-

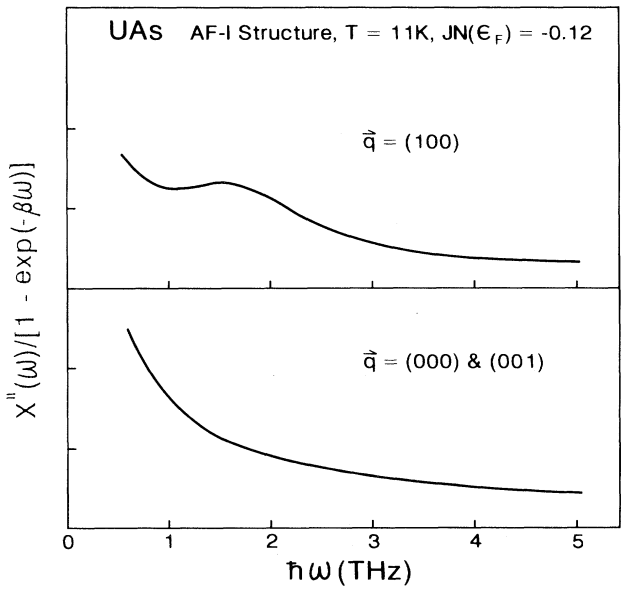

FIG. 3. Calculated imaginary part of the dynamic susceptibility $\chi''(\omega)$ vs energy $\hbar\omega$ for the AF-I phase of UAs at $T=11$ K at the zone center $\mathbf{q}=(000)$ and zone boundaries (001) and (100). The range parameters are $E_2=E_1$, $E_3=-0.5E_1$ ($E_1=500$ K to match $T_N=127$ K); the crystal-field parameters are $W=-0.02E_1$, $x=1$; the dynamic parameter $\delta N(\varepsilon_F)=-0.12$.

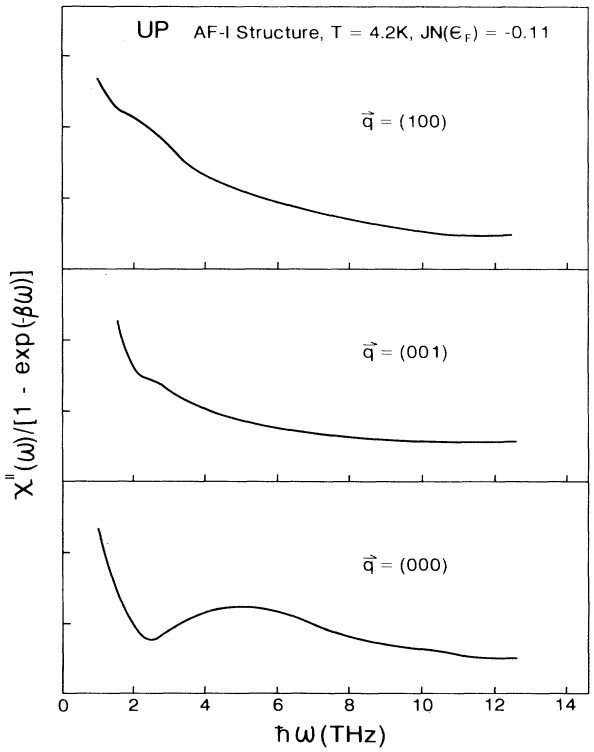

FIG. 4. Calculated imaginary part of the dynamic susceptibility $\chi''(\omega)$ vs energy $\hbar\omega$ for the AF-I phase of UP at $T=4.2$ K at the zone center $\mathbf{q}=(000)$, and at the zone boundaries (001) and (100). The range parameters are $E_2=E_1$, $E_3=-0.6E_1$ ($E_1=215.5$ K to match experimental $T_N=125$ K); the crystal-field parameters are $W=-0.05E_1$, $x=1$; and the dynamic parameter $\delta N(\varepsilon_F)=-0.11$.

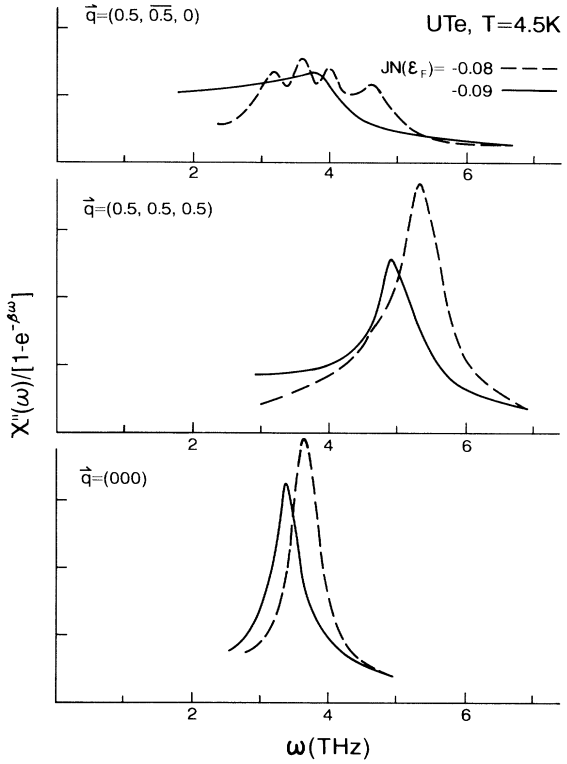

FIG. 5. Calculated imaginary part of the dynamic susceptibility $\chi''(\omega)$ vs energy $\hbar\omega$ for ferromagnetic UTe at $T=4$ K at the $(\mathbf{q}=0)\Gamma$ point and at $q=0.5$ along both $[qqq]$ and $[q\bar{q}0]$. The range parameters are $E_2=E_1$, $E_3=-0.5E_1$ ($E_1=150$ K to match the experimental $T_c=104$ K); the crystal-field parameters $W=0.005E_1$ and $x=1$; and the dynamic parameter $\delta N(\varepsilon_F)=-0.08$.

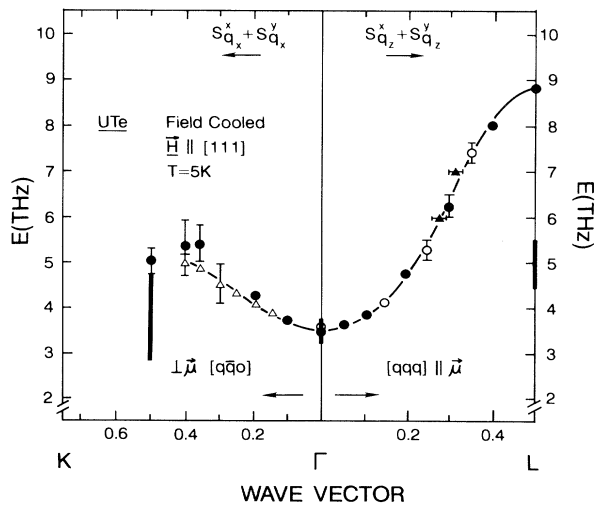

FIG. 6. The three vertical bars show our calculated excitation energies and half widths superimposed on the experimental dispersion behavior found by Lander *et al.* (Fig. 6 of Ref. 18) for UTe.

lated broadened excitation energies compared to the experimental overall dispersion of Ref. 18 in Fig. 6). At $T=4.5$ K the calculated excitation energy is 3.4 THz and the linewidth is ~ 0.6 THz at the zone center; along the $[qqq]$ direction the energy rises to 5.0 THz, and the linewidth increases to ~ 1 THz at the zone boundary $q=0.5$; while in the $[q\bar{q}0]$ direction the calculated width of the excitations increases very rapidly to greater than 2 THz, but the excitation energy increases only a moderate amount to ~ 3.8 THz at $q=0.5$. These results (the calculated shape of the dispersion curve and the linewidths) are in good agreement with the experimental results of Lander *et al.*[18] As can be seen in Fig. 6, the anisotropy of the broadening is captured quite well; and the only discrepancy between our calculated excitation behavior and the observed excitation behavior at low temperature is that the predicted energy increase is not as rapid as observed on going from Γ to the zone boundary.

To understand why a distinguishable excitation occurs only at the Γ point for UP and only at $\mathbf{q}=(100)$ for UAs, but not anywhere else in the Brillouin zone, we carefully examined the predamping excitation modes. We found that because of the strong anisotropic hybridization-mediated two-ion interactions, which remove the degeneracy of the crystal-field states to form a complicated 10-energy-level system and yield a strongly anisotropic excitation dispersion (strongly $\mathbf{q}$ dependent), along certain directions and for certain values of $\mathbf{q}$ there is only one intense excitation, while outside these certain regions of $\mathbf{q}$ space there may exist two or more intense modes sharing intensity. In the former cases, no matter how large the damping effect is [how large the value of $\delta N(\varepsilon_F)$ is chosen] one can always identify a broad excitation, but in the latter cases, if these intense modes are close enough in energy, the broadening effect will cause the overlap of peaks. In that case the relatively large value of $\delta N(\varepsilon_F)$ washes out all the peaks and yields a continuous response. The same thing happens in the magnetic excitation spectrum in UTe. The broad response at $q=0.5$ along the $[q\bar{q}0]$ direction is actually a composition of four peaks which share the intensity and happen to be close enough in energy so that the large damping effect washes out these peaks, and the final linewidth is essentially the summation of the widths of four peaks. On the other hand, going across the Brillouin zone from the Γ point to the boundary along the $[qqq]$ direction there is only one intense mode, and the moderate increase in the linewidth in this direction comes merely from the increase of the excitation energy but not from the overlap of peaks.

The value of the crystal-field parameter W plays a crucial role in the behavior just described for UTe. For positive values of W ranging from $0.001E_1$ to $0.01E_1$, giving a crystal-field quartet ground state, the calculated energy, linewidth, and dispersion of excitations are almost the same. They are all in good agreement with the experiment. But for any negative W, which yields a Γ_6 doublet ground state if there is no two-ion interaction, no matter what values of E_1, E_2, E_3, and $\delta N(\varepsilon_F)$ are chosen, we can never bring the intense modes close enough to form a broad peak at $\mathbf{q}=(0.5,-0.5,0)$, and an excitation spec-

trum with multiple peaks, which is not in agreement with experiment, is obtained.

From the above discussion we conclude that (1) the crystal-field splitting in UTe must be a positive value (Γ_8 quartet rather than Γ_6 doublet crystal-field ground state), and (2) the complex behavior of the magnetic excitations is closely related to the physical picture involving the two-ion interactions and the crystal-field interactions as defined through the parameters E_1, E_2, E_3, and W (or B_4). One can see how in the absence of this physical picture and description, one has the usual situation where a different set of parameters must be used in the static and in the dynamic calculations to get good theoretical agreement with experiment. Thus, it is important to note that in our cases only one set of parameters is used for both static and dynamic calculations [one additional parameter $\mathcal{J}N(\varepsilon_F)$ is used in the dynamic calculations], and our results are nevertheless in excellent agreement with both the static and the dynamic experiments.

In our relaxation calculations we choose the values of $\mathcal{J}N(\varepsilon_F)$ to fit the observed linewidths at the Γ point. The values are $-0.08--0.09$ for CeSb, CeBi, and PuSb, and $-0.11--0.12$ for UP and UAs (about 40% larger than in Ce^{3+} and Pu^{3+}). In Sec. II, we have pointed out that if we consider the physical picture associated with the Schrieffer-Wolff transformation, the value of $\mathcal{J}$ would be expected to increase dramatically as we move from Ce^{3+} and Pu^{3+} to U^{3+} as the energy difference between the f levels and the Fermi energy undergoes a large decrease ($\mathcal{E}_f \sim 2$ eV for Ce^{3+} and Pu^{3+}, and ~ 0.5 eV for UP and UAs). However, the direct Hamiltonian term causes a broadening of the f levels which tends to reduce $\mathcal{J}$. The net effect yields an almost constant value of $\mathcal{J}$. The 40% increase in the phenomenological input value of $\mathcal{J}N(\varepsilon_F)$ for UP and UAs might come from the increase of the density of states $N(\varepsilon_F)$. Since we expect a larger $\mathcal{E}_f$ value for UTe which has a larger lattice parameter than UP and UAs, $\mathcal{J}N(\varepsilon_F)$ of -0.09 is a reasonable choice for UTe according to the above analysis. Our recent *ab initio* calculation[44] agrees with this phenomenologically derived value.

Contrary to the unchanged $\mathcal{J}N(\varepsilon_F)$ for PuSb and the moderate ($\sim 40\%$) increase in $\mathcal{J}N(\varepsilon_F)$ for UP and UAs compared to Ce^{3+}, we have over six and ten or more times larger two-ion interactions for PuSb, UTe and for UP, UAs, respectively. By choosing the range parameter E_1 which characterizes the two-ion interactions to match the experimental values of the transition temperatures we have $E_1 = 15.35$ K for CeSb, 18.94 K for CeBi, 121 K for PuSb, 150 K for UTe, 215.5 K for UP, and 500 K for UAs. This discrepancy between the moderate increase in $\mathcal{J}N(\varepsilon_F)$ and the dramatic increase in E_1 can be understood as follows. According to the first-principles calculations by Wills and Cooper,[6] for $Ce^{3+}(4f^1)$ systems to fourth order in H_2 the range functions $E(\mathbf{R})$ are given by

$$E(M_2',M_2;M_1',M_1;\mathbf{R}) = -\sum_{\varepsilon_k < E_F}\sum_{\varepsilon_k' > E_F} \frac{[\mathcal{J}^{M_2'M_2}(\mathbf{k}',\mathbf{k})]^* \mathcal{J}^{M_1M_1'}(\mathbf{k}',\mathbf{k})}{\varepsilon_k - \varepsilon_{k'}} e^{-i(\mathbf{k}-\mathbf{k}')\cdot\mathbf{R}} \tag{4.1}$$

with

$$\mathcal{J}^{MM'}(\mathbf{k},\mathbf{k}') = j_{N-1}^{MM'}(\mathbf{k},\mathbf{k}') - j_N^{MM'}(\mathbf{k},\mathbf{k}') \ . \tag{4.2}$$

The range functions depend not only on $\mathcal{J}$ through the numerator in Eq. (4.1), but also through the denominator on the detailed band structure throughout the whole Brillouin zone. To order $(H_2)^4$, both in the Schrieffer-Wolff transformation theory and in the perturbation in Eqs. (2.4)–(2.8), Wills and Cooper[6] have obtained for Ce^{3+} systems a quite complicated expression for the range functions [Eq. (2.8) in Ref. 6]. For $Pu^{3+}(5f^5)$ and $U^{3+}(5f^3)$ systems, according to the discussion given in Sec. II, we expect the same expression for the range functions. Then, the more dramatic increase in the value of E_1 than in the value of $\mathcal{J}N(\varepsilon_F)$ for Pu^{3+} and U^{3+} systems [compared to E_1 and $\mathcal{J}N(\varepsilon_F)$ for Ce^{3+} systems] reflects the differences of the band structures between these systems, especially with regard to the density of f states at ε_F (resulting from increased f-f overlap). Further, first-principles calculations of the range functions for Pu^{3+} and U^{3+} systems would be valuable.

V. SUMMARY

In conclusion, we have found the following for the Ce^{3+}, Pu^{3+}, and U^{3+} systems: (1) To fully understand the unusual magnetic behaviors, besides the hybridization dressed crystal-field interactions and the hybridization-mediated two-ion interactions which are the main mechanism for the strong magnetic anisotropy existing in these systems, one has to include in the calculation the relaxation effects caused by the single-site hybridization of the band electrons with f electrons. (2) For CeSb and CeBi the relaxation effects dramatically change the shapes of the magnetic excitation dispersion curves especially for the wave vector $\mathbf{q}$ along the [001] direction (perpendicular to the ordered moment). After including the damping and shifts of the magnetic excitations, the similarity of the dispersion curves between CeSb and CeBi can be understood although their static properties (such as the phase diagrams) and the crystal-field splittings, are quite different. (3) For PuSb the damping and shift effects change neither the dispersion nor the polarization of the modes. The relaxation basically results only in an overall shift of the excitation energies. The fine tuning of the calculated excitation behavior provided by the damping does not capture the final subtle changes needed for full agreement with experiment. (4) On the other hand, the agreement in subtle detail of theory and experiment for the uranium compounds provided by including the single-site hybridization damping is remarkably good. The unusual observed broad continuum magnetic excitation response in UP and UAs, and the very strong anisotropy of both the dispersion and the damping of the exci-

tations for UTe, can be understood only after including the damping of normal modes. The predicted results are in very good agreement with the experiments. (5) The fact that there is almost no change in the values of the single-ion hybridization strength parameter Δ as we move from Ce^{3+} systems to U^{3+} can be understood by the renormalization effect by the direct Hamiltonian term of Eq. (2.6); while the dramatic increase in value of the range parameter E_1 is believed to come from the large differences of the band structures (increased f-f overlap) between these systems.

ACKNOWLEDGMENTS

This research was supported by U.S. DOE Grant No. DE-FG05-89ER45386 and by a grant from the European Institute for the Transuranium Elements. We have especially benefited from continued encouragement and much valuable detailed discussion of the experiments from G. H. Lander. We are also indebted to W. J. L. Buyers and J. Rossat-Mignod for much valuable discussion and encouragement.

[1]B. R. Cooper and R. Siemann, J. Appl. Phys. **50**, 1991 (1979); R. Siemann and B. R. Cooper, Phys. Rev. Lett. **44**, 1015 (1980).

[2]B. R. Cooper, R. Siemann, D. Yang, P. Thayamballi, and A. Banerjea, in *Handbook on the Physics and Chemistry of the Actinides,* edited by A. J. Freeman and G. H. Lander (North-Holland, Amsterdam, 1985), Chap. 6, pp. 435–500.

[3]P. Thayamballi, D. Yang, and B. R. Cooper, Phys. Rev. B **29**, 4049 (1984).

[4]P. Thayamballi and B. R. Cooper, J. Appl. Phys. **55**, 1829 (1984); Phys. Rev. B **31**, 6004 (1985).

[5]G. J. Hu, N. Kioussis, A. Banerjea, and B. R. Cooper, Phys. Rev. B **38**, 2639 (1988).

[6]J. M. Wills and B. R. Cooper, Phys. Rev. B **36**, 3809 (1987).

[7]N. Kioussis, B. R. Cooper, and A. Banerjea, J. Appl. Phys. **61**, 3388 (1987); Phys. Rev. B **38**, 9132 (1988).

[8]G. J. Hu and B. R. Cooper, J. Appl. Phys. **63**, 3826 (1988).

[9]G. J. Hu and B. R. Cooper, J. Appl. Phys. **64**, 5592 (1988).

[10]G. J. Hu and B. R. Cooper, Phys. Rev. B **38**, 9127 (1988).

[11]H. Heer, A. Furrer, W. Halg, and O. Vogt, J. Phys. C **12**, 5207 (1979).

[12]J. Rossat-Mignod, J. M. Effantin, P. Burlet, T. Chattopadhyay, L. P. Regnault, H. Bartholin, C. Vettier, O. Vogt, D. Ravot, and J. C. Achart, J. Magn. Magn. Mater. **52**, 111 (1985).

[13]J. Rossat-Mignod, P. Burlet, S. Quezel, and O. Vogt, Physica (Utrecht) **102B+C**, 237 (1980).

[14]W. J. L. Buyers and T. M. Holden, in *Handbook on the Physics and Chemistry of the Actinides,* edited by A. J. Freeman and G. H. Lander (North-Holland, Amsterdam, 1985), Chap. 4.

[15]W. G. Stirling, G. H. Lander, and O. Vogt, Physica **102B+C**, 249 (1980).

[16]G. H. Lander and W. G. Stirling, Phys. Rev. B **21**, 436 (1980).

[17]T. M. Holden, W. J. L. Buyers, E. C. Svensson, and G. H. Lander, Phys. Rev. B **30**, 114 (1984).

[18]G. H. Lander, W. G. Stirling, J. W. Rossat-Mignod, M. Hagen, and O. Vogt, Physica B **156-157**, 826 (1989); Phys. Rev. B **41**, 6899 (1990).

[19]G. H. Lander, A. Delapalme, P. J. Brown, J. C. Spirlet, J. Rebizant, and O. Vogt, Phys. Rev. Lett. **53**, 2262 (1984); J. Appl. Phys. **57**, 3748 (1985); P. Burlet, S. Quezel, J. Rossat-Mignod, J. C. Spirlet, J. Rebizant, W. Muller, and O. Vogt, Phys. Rev. B **30**, 6660 (1984).

[20]G. H. Lander, W. G. Stirling, J. Rossat-Mignod, J. C. Spirlet, J. Rebizant, and O. Vogt, Physica B **136**, 409 (1986).

[21]H. Mori, Prog. Theor. Phys. (Kyoto) **33**, 423 (1965); D. Forster, *Hydrodynamics, Fluctuations, Broken Symmetry and Correlation Functions* (Benjamin, Reading, MA, 1975), Chap. 5; E. Fick and G. Sauermann, *The Quantum Statistics of Dynamic Processes* (Springer, Berlin, 1990), Chap. 11.

[22]M. Campagna, G. K. Wertheim, and Y. Baer, in *Photoemission in Solids (II),* edited by L. Ley and M. Cardona (Springer, Berlin, 1979), Chap. 4, pp. 217–260.

[23]J. R. Schrieffer, J. Appl. Phys. **38**, 1143 (1967); J. R. Schrieffer and P. A. Wolff, Phys. Rev. **149**, 491 (1966).

[24]B. Coqblin and J. R. Schrieffer, Phys. Rev. **185**, 847 (1969).

[25]B. Cornut and B. Coqblin, Phys. Rev. B **5**, 4541 (1972).

[26]M. A. Ruderman and C. Kittel, Phys. Rev. **96**, 99 (1954); T. Kasuya, Prog. Theor. Phys. **16**, 45 (1956); K. Yosida, Phys. Rev. **106**, 893 (1957).

[26a]B. R. Cooper, Q. G. Sheng, and S. P. Lim, J. Alloys Compounds **192**, 223 (1993).

[26b]N. Kioussis, B. R. Cooper, and J. M. Wills, Phys. Rev. B **44**, 10 003 (1991).

[26c]B. R. Cooper, Q. G. Sheng, S. P. Lim, C. Sanchez-Castro, N. Kioussis, and J. M. Wills, J. Magn. Magn. Mater. **108**, 10 (1992).

[27]M. Tinkham, *Group Theory and Quantum Mechanics* (McGraw-Hill, New York, 1964), Chap. 5.

[28]J. Kondo, Solid State Phys. **23**, 183 (1969).

[29]G. Toulouse and B. Coqblin, Solid State Commun. **7**, 853 (1969).

[30]K. W. Stevens, Prog. Phys. Soc. London, Sect. A **65**, 209 (1956); M. T. Hutchings, in *Solid State Physics,* edited by F. Seitz and D. Turnbull (Academic, New York, 1964), Vol. 16, pp. 227–273.

[31]K. R. Lea, M. J. M. Leask, and W. P. Wolf, J. Phys. Chem. Solids **23**, 1381 (1962).

[32]K. W. Becker, P. Fulde, and J. Keller, Z. Phys. B **28**, 9 (1977).

[33]G. J. Hu and D. L. Huber, Phys. Rev. B **31**, 927 (1985).

[34]R. J. Birgeneau, E. Bucher, J. P. Maita, L. Passel, and K. C. Turberfirld, Phys. Rev. B **8**, 5345 (1973).

[35]G. Busch and O. Vogt, Phys. Lett. **25A**, 449 (1967).

[36]B. R. Cooper, M. Landolt, and O. Vogt, in *Proceeding of the International Conference on Magnetism ICM-73,* edited by R. P. Ozerov and Yu. A. Izyumov (Nauka, Moscow, 1974), Vol. 5, pp. 354–360.

[37]J. W. Cable and W. C. Koehler, *Magnetism and Magnetic Materials 1971 (Chicago),* Proceedings of the 17th Annual Conference on Magnetism and Magnetic Materials, AIP Conf. Proc. No. 5, edited by D. G. Graham and J. J. Rhyne (AIP, New York, 1972), p. 1381.

[38]J. Rossat-Mignod, P. Burlet, J. Villain, H. Bartholin, T. S. Wang, D. Florence, and O. Vogt, Phys. Rev. B **16**, 440 (1977).

[39]P. Fischer, B. Lebech, G. Meier, B. D. Rainford, and O. Vogt,

J. Phys. C **11**, 345 (1978).
[40]J. Rossat-Mignod, P. Burlet, J. Quezel, J. M. Effantin, D. Delacote, H. Bartholin, O. Vogt, and D. Ravot, J. Magn. Magn. Mater. **31-34**, 398 (1983).
[41]B. Halg and A. Furrer, J. Appl. Phys. **55**, 1860 (1984).
[42]A. Banerjea, B. R. Cooper, and P. Thayamballi, Phys. Rev. B **30**, 2671 (1984).
[43]G. Gilat and N. R. Bharatiya, Phys. Rev. B **12**, 3479 (1975).
[44]G. J. Hu and B. R. Cooper, J. Appl. Phys. **67**, 5197 (1990).